ISIJ International, Vol. 46 (2006), No. 1, pp. 138–146

Tempering Kinetics of the Martensitic Phase in DP Steel

T. WATERSCHOOT,[1] K. VERBEKEN[2] and B. C. DE COOMAN[1]

1) Laboratory for Iron and Steelmaking, Department of Metallurgy and Materials Science, Ghent University (UGent), Technologiepark 903, B-9052 Gent (Zwijnaarde), Belgium. E-mail: Bruno.DeCooman@UGent.be
2) Fund for Scientific Research-Flanders (Belgium) (F.W.O.-Vlaanderen).

(*Received on July 8, 2005; accepted on October 26, 2005*)

The increase in the yield stress of dual phase (DP) steels, resulting from the static strain ageing phenomenon, commonly referred to as bake hardening (BH), gives an important contribution to the additional in-service strength of outer auto body parts, *e.g.* with respect to the dent resistance of the components made with DP steel. In order to understand this large BH effect, the role of the different constituents of the DP steel during this process needs to be considered. The various stages of tempering phenomena taking place in the martensite phase were investigated in detail by means of precision dilatometry and X-Ray Diffraction (XRD). The succession of the various tempering reactions that are characterised by typical volume changes was determined using both constant heating rate and isothermal dilatometric tests. The measurements made it possible to distinguish five distinct stages of structural changes during tempering: (I) the redistribution of carbon atoms, (II) the precipitation of η- or ε-carbide, (III) the formation of Hägg-carbide, (IV) the decomposition of retained austenite, and (V) the transformation of transition carbides to cementite.

KEY WORDS: bake hardening; dual phase steel; tempering; martensite; XRD, dilatometry.

1. Introduction

The pure dual phase (DP) microstructure consists of a matrix of soft α-ferrite grains, strengthened by a finely dispersed, hard MA (Martensite–Austenite) constituent (**Fig. 1**). The volume fraction of martensite mainly determines the strength of DP steel and typically varies between 5 and 50 %. In DP steels used for structural parts of a car body the volume fraction of martensite is typically between 10 and 15 %. The steel obtains its specific properties from the low temperature transformation of intercritical austenite to lath-type martensite. This transformation results in a non-uniform dislocation distribution and internal stresses. The austenite, enriched in carbon during the processing, may not transform entirely into martensite, resulting in the presence of small amounts of retained austenite. The amount of retained austenite depends among others, on the hardenability of the transforming austenitic phase and the size of the austenitic particles. For most industrially processed DP steels, the presence of small amounts of other constituents, such as bainite and, to a lesser degree, pearlite, can be tolerated as these do not significantly alter the specific dual phase properties as long as a sufficient amount of low-temperature martensite has been formed. At low strains, DP steel exhibits a lower yield stress, a continuous yielding and an increased strain hardening rate when compared to steels with a mainly ferritic microstructure such as IF steels and HSLA steels. The lack of a yield point eliminates the risk of Lüders-band formation and ensures that a good surface finish is obtained after press forming, *i.e.* the absence of 'orange peel'-like surface defects on pressed panels.

DP steels are characterized by a large increase in yield strength after low temperature annealing of prestrained samples, *i.e.* after bake hardening (BH). This increase in yield stress gives an important contribution to the additional in-service strength with respect to the dent resistance of the components made out of this steel when they are applied for outer body parts. The understanding of this large bake hardening effect, which is a static strain ageing phenomenon, requires the study of the mechanism of the ageing process with specific reference to the contribution from the different constituents and their role on the overall strengthening behavior.

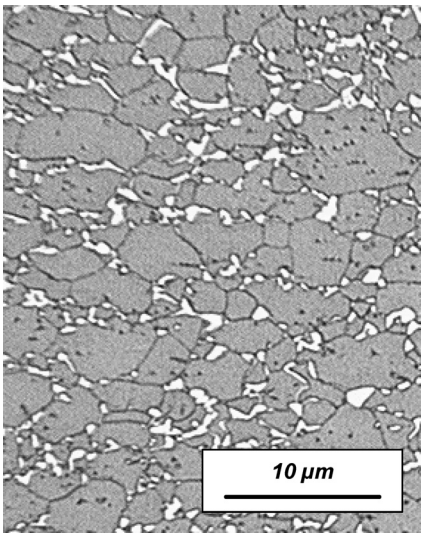

Fig. 1. Microstructure of DP steel.

However, no specific research has yet been reported on the fundamental mechanisms occurring in the martensitic phase during the bake hardening of DP steel. Unlike the ELC (Extra Low Carbon, C∼200 ppm) and ULC (Ultra Low Carbon, C<50 ppm) steels,[1,2] where ageing phenomena are principally guided by the amount of interstitial carbon atoms, the dislocation density and the ferrite grain size, the bake hardening in DP steel is expected to be more complex in nature, as a result of its two phase microstructure. The low temperature bake hardening process indeed causes both static strain ageing phenomena in the ferrite and tempering phenomena in the martensite. In the ferritic phase, the bake hardening mechanism is influenced by the interstitial carbon content, the carbon in the grain boundaries, the specific distribution of the dislocations and residual stresses, and possibly by carbon released from the martensite as a result of tempering phenomena. In the lath-type martensite, present in DP steels, analogous processes will occur, but, in addition, there will be a volume contraction of martensite during tempering, changes in the martensitic strength, additional carbon clustering or precipitation near the ferrite/martensite interfaces and effects related to the presence of retained austenite. The processes are expected to overlap at higher ageing temperatures.

Waterschoot *et al.*[3,4] have described the bake hardening behavior of dual phase steels by means of internal friction measurements and neutron diffraction. They observed distinct strengthening stages which they ascribed to Cottrell atmosphere formation, precipitation and strengthening due to tempering processes in the martensite. The Cottrell atmosphere formation was revealed by the strain hardening behavior of the aged samples; it had a $t^{2/3}$ kinetic law in correspondence with the ageing kinetics proposed by Cottrell.[5] The high dislocation density and the large number of dislocation–dislocation interactions in the DP steels created numerous precipitation sites. The presence of abundant nucleation sites stimulated carbon clustering and carbide precipitation in the ferrite. This was considered to be responsible for the significant increase in the yield stress after the Cottrell atmosphere formation. The magnitude of the strengthening due to precipitation was found to depend on the interstitial carbon content of the initial matrix.

The strengthening that occurred during the tempering of martensite was studied by internal friction measurements on the samples aged for times beyond the completion of the precipitation stage. These measurements did not reveal the presence of any interstitial carbon in the ferrite matrix. The volume decrease of the martensite due to the formation of carbon clusters and/or transition carbides reduced the internal stresses in the ferrite. In combination with the presence of pinned dislocations in the ferrite matrix, this resulted in a large increase of the yield strength. The tempering of the martensite was also indicated by a decrease in the tensile strength of the aged samples. The highest increase in the yield stress was observed for the samples with the largest volume fraction of martensite. The solute carbon content was found to play an important role in the ageing behavior of dual phase steels. An increased amount of interstitial carbon shortens the incubation time and increases the yield stress.

In order to obtain a better understanding of the dual phase ageing behavior, the various stages of the tempering of the isolated martensite phase of dual phase steels was studied in greater detail by means of precision dilatometry and XRD measurements. Using both constant heating rate and isothermal dilatometric tests, the succession of the various tempering reactions, which lead to characteristic volume changes, was determined. The XRD measurements resulted in additional information about the stages involved in the tempering process.

The evaluation of kinetic reaction parameters, in particular the activation energy, can be performed by investigating the change in physical properties that reflect the course of the transformation. The property that is considered in this work is the change of the specific volume obtained from the dilatational length changes. The transformed fraction, f, is defined as:

$$f = \frac{l - l_0}{l_1 - l_0} \quad \text{.....(1)}$$

Where l indicates the length of the sample, and l_0 and l_1 the initial and final sample length, *i.e.* before and after the transformation. For non-isothermal annealing experiments, l_0 and l_1 depend on the temperature, the rate and the amount of transformation. In isothermal conditions a heterogeneous solid-state transformation can often be described by means of the Johnson–Mehl–Avrami (JMA) equation:

$$f = 1 - \exp(-\beta^n) \quad \text{.....(2)}$$

with

$$\beta = k(T) \cdot t = k_0 \cdot \exp\left(-\frac{Q}{R \cdot T}\right) \cdot t \quad \text{.....(3)}$$

Where Q is the activation energy, k_0 is a constant, T is the temperature (K), t is the time (s), R is the gas constant (8.314 J/mol·K) and n is the time exponent, which usually remains constant at different temperatures for a specific transformation.

The mathematics for the application of the JMA equation in case of non-isothermal annealing were developed by Mittemeijer *et al.*[6–9] For annealing with a constant heating rate, Φ (K/min), the following formula can be derived:

$$\beta = \int_0^t k(T(t))dt \approx k_0 \cdot \frac{R}{Q} \cdot \frac{T^2}{\Phi} \quad \text{.....(4)}$$

Using Eqs. (1), (2) and (4) a relation between the specific volume of the sample and the kinetic parameters Q, n and k_0 can be obtained. An easily accessible experimental quantity is the temperature T_i corresponding to the inflection point of the sample length *vs*. T curve obtained from dilatometry. It has been shown that[6]:

$$\ln\left(\frac{T_i^2}{\Phi}\right) \approx \frac{Q}{R \cdot T_i} + \ln\left(\frac{Q}{R \cdot k_0}\right) \quad \text{.....(5)}$$

The activation energy Q can, therefore, be derived from the slope of the straight line obtained by plotting $\ln(T_i^2/\Phi)$ *vs.* $1/T_i$ for different values of Φ.

Table 1. Chemical composition of the investigated material.

	C %	Mn %	Si %	Cr %	Mo %	α_M vol%	M_s °C	γ_{ret} vol%	C_i ppm	C_{α_M} mass%
DP steel	0.08	1.50	0.13	0.36	0.21	12	-	2.6	3	0.59
α_M	0.72	1.53	0.11	0.28	0.20	88	195	12	-	0.70

2. Experimental

The composition of a standard CMnCrMo DP steel is shown in **Table 1**. In order to study the intrinsic properties of the martensitic phase separately, a laboratory casting was done with the composition corresponding to that of the carbon enriched martensite. The composition of this martensitic casting is also given in Table 1. Before hot rolling, laboratory cast blocks of the martensitic material were reheated to 1 250°C for 1 h. The dilatometric samples were prepared from a 6 mm thick hot rolled and air cooled sheet. The samples were heated to 900°C for 5 min in a salt bath furnace, water quenched in order to obtain a fully martensitic structure, and kept at a constant temperature of 4°C until testing. The same material was also used for the XRD-measurements.

The tempering phenomena and phase transformations were experimentally studied by means of dilatometry and XRD-measurements. Dilatometry is based on the monitoring of the change in length of a sample during heating, cooling or isothermal holding. By consequence, this technique monitors the volume change occurring during the transformation or tempering. Martensite has a larger specific volume than ferrite because of its body centered tetragonal lattice. As the martensite lattice evolves towards body centered cubic during tempering, a volume decrease will occur. The austenite crystal structure has a higher density than the ferrite crystal structure. In pure iron, the $\gamma \rightarrow \alpha$ transformation implies a volume expansion of 1.03 %. The dilatometry equipment used was an automated Theta Dilatronic IIIS quench dilatometer. The dilatometry samples were solid cylindrical specimens with 3.5 mm diameter and 5 mm length.

XRD-measurements were performed on a Siemens D5000 Diffraktometer using MoK_α radiation ($\lambda = 0.0711$ nm). The volume fraction of retained austenite was determined using the Direct Comparison Method.[10]

3. Results

Internal friction measurements on the martensitic material, which were extensively commented in earlier work,[3] did not result in a significant Snoek-type damping peak. Results from Speich *et al.*[11–13] confirmed that the carbon in martensite does not result in a low temperature Snoek-type internal friction peak, which implies that the carbon atoms tend to remain in an ordered array (Zener ordering).

Previous neutron diffraction measurements[4] revealed 12 vol% of retained austenite in the martensitic material. Measurements on DP steel also confirmed the observation made on the isolated martensite; small amounts of retained austenite were usually found, typically 0.7–2.6 vol%. By consequence, it was concluded that the martensitic transformation was not complete at room temperature, due to its low transformation rate. The martensite and retained austenite lattice parameters were also determined. The retained austenite lattice parameter a_γ was equal to 0.3593 nm. The martensite lattice parameters, a_{α_M} and c_{α_M}, were 0.2860 and 0.2944 nm, respectively. Tempering of the martensite for 1 h at 100°C only caused a small decrease of the $c_{\alpha_M}/a_{\alpha_M}$ ratio. After tempering for 5 h at 170°C the $c_{\alpha_M}/a_{\alpha_M}$ ratio decreased rapidly and clear η-carbide diffraction peaks were observed. In addition, a small increase of the austenite lattice parameter was noticed, strongly suggesting the relaxation of internal compressive stresses. After ageing at 350°C, the martensitic material had a bcc structure and the low temperature transition carbides were replaced by cementite precipitates.

In the course of the present work, the martensitic transformation was characterized by reheating dilatometric samples to 900°C for 5 min and by fitting the cooling dilatation curve obtained during air quenching to the Koistinen–Marburger equation.[14] The martensitic start temperature, M_s, is determined as a parameter of the linear fitting of $-\ln(1-f_M)$ *vs.* the temperature. The transformation rate, α, appears to be low due to the high carbon content. The experimentally measured M_s temperature was 195°C. Using the linear expansion, $\Delta l/l_0$, the volume expansion associated with the martensitic transformation, $\Delta V/V_0 \approx 3 \cdot \Delta l/l_0$, was experimentally found to be ~2.1 vol%. The martensitic transformation was not completed at room temperature, an observation which confirmed earlier neutron diffraction measurements.

Figure 2 shows a characteristic dilatometric curve for a tempering treatment at 5°C/min. A clear shift of the inflection points, corresponding to the tempering phenomena, to higher transformation temperatures was observed for higher heating rates. In the present work dl_T/l_0, was used rather than f in Eq. (2). In this case, dl_T represents the deviation from the ideal thermal expansion due to tempering. It is the length change associated with the tempering processes occurring in the material. In order to determine the position of the inflection points accurately, the first derivate of the length change was plotted as a function of the temperature (Fig. 2(c)).

Five stages could be distinguished during the tempering of the martensite. The activation energy of the different processes was determined using $\ln(T_i^2/\Phi)$ *vs.* $1/T_i$ graphs, in which the slope of the lines was used to determine the activation energy (**Fig. 3**). An overview of the activation energies and the corresponding tempering processes and temperature ranges is listed in **Table 2**. Based on the present knowledge[8] about tempering phenomena in martensite, these stages were identified as (I) the redistribution of car-

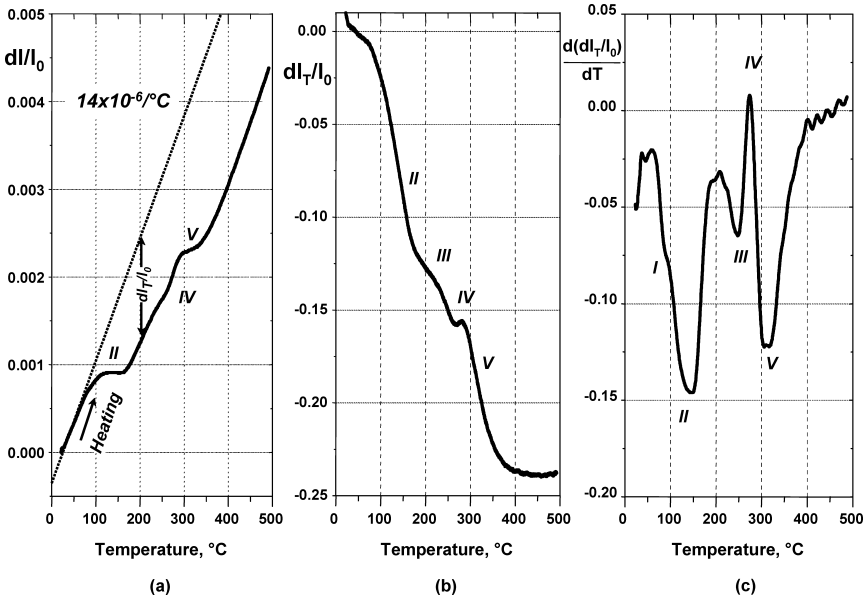

Fig. 2. Dilatometer curve for the bulk martensite similar to the martensite present as a dispersed phase in the DP steel. The material was heated from 20 to 500°C at a constant heating rate of 5°C/min; (a) the length change of the material due to tempering (b) and the derivative length change as a function of the temperature (c).

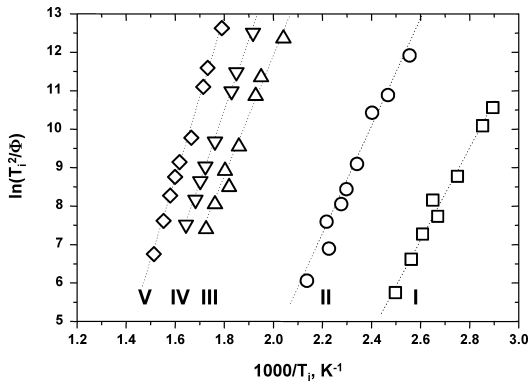

Fig. 3. The $\ln(T_i^2/\Phi)$ *vs.* $1/T_i$ plot for the determination of the activation energy of the different tempering stages based on Eq. (6).

Table 2. Activation energy data for the different martensite tempering stages.

	Process	Activation Energy (Q)	Temperature range
I	Segregation of C to lattice defects	100.6 kJ/mol	60-120°C
II	Precipitation of η-carbide	123.8 kJ/mol	120-195°C
III	Precipitation of Hägg-carbide	135.8 kJ/mol	220-300°C
IV	Transformation of retained γ	154.7 kJ/mol	250-350°C
V	Precipitation of cementite	176.1 kJ/mol	290-390°C

bon atoms, (II) the precipitation of the η-transition carbide, (III) the formation of Hägg-transition carbides, (IV) the transformation of retained austenite and (V) the precipitation of cementite.

The stage I tempering phenomenon occurs in the 60–120°C temperature range and results in a minor volume decrease of less than 0.05 vol%. Two pre-precipitation low-temperature ageing processes are usually distinguished a segregation of interstitial carbon to lattice defects such as lath boundaries and dislocations, and clustering of the interstitial carbon atoms. It has been suggested[9,12] that dislocations and boundaries are saturated at about 0.2 wt% C. The carbon segregation causes a small decrease in volume and is thus expected to be the reason for the initial decrease in sample length. Furthermore, it reduces c_{α_M}. The majority of the carbon atoms are involved in the clustering, which results in a modulated structure, referred to as "Tweed" in transmission electron microscopy observations. In carbon-rich steels, *i.e.* 1 wt% C or more, a clear separation between the clustering and ordening of carbon atoms has been reported.[15] Streaks in the electron diffraction pattern, obtained by TEM, are observed when only clustering has occurred. When ordening has taken place as well, additional satellite diffraction spots are observed. Observation of these features in an electron diffraction pattern is believed to be very unlikely in the present case due to the much lower carbon content of the investigated steels. During the initial clustering stages, the tetragonality of the martensite is constant. Later on, cluster coarsening causes larger regions of the martensitic lattice to become depleted in carbon, resulting in a low-tetragonality martensite. The activation energy of the segregation process was determined to be 100.6 kJ/mol from Fig. 3.

Stage II is characterized by a volume decrease of about 0.30 vol% occurring in the 120–195°C temperature range. In earlier studies,[16–19] it has been referred to as the first stage of tempering. The volume decrease is due to the formation of the transitional orthorhombic η-carbide Fe_2C and/or the hexagonal ε-carbide $Fe_{2.4}C$. In this stage the tetragonality of the martensite, *i.e.*, its $c_{\alpha_M}/a_{\alpha_M}$ ratio, decreases as multiplets coarsen to form η- and/or ε-carbide precipitates, and results in a measurable volume decrease. The measured activation energy of 123.8 kJ/mol, which is in good agreement with the activation energies in the 111–126 kJ/mol range, reported by Cheng *et al.*[9] for 1.1 mass% C martensite.

Stage III and IV both occur in the same temperature

Table 3. Heat treatments in order to obtain the XRD samples for different tempering stages.

	Phenomenon	Heat treatment	Changes in diffractogram
WQ	Water quenched martensite	-	-
AQ	Air quenched martensite	-	auto-tempering
I	Segregation of C to lattice defects	1 day, 70°C	Small decrease of $c_{\alpha_M}/a_{\alpha_M}$
II	Precipitation of η-carbide	1 day, 150°C	$c_{\alpha_M}/a_{\alpha_M} \sim 1$
III	Precipitation of Hägg-carbide	2 hours, 200°C	Decrease FWHM α_M peak
IV	Transformation of retained γ	2 hours, 250°C	γ_{ret} peaks disappear
V	Precipitation of cementite	2 hours, 350°C	γ_{ret} peaks disappear

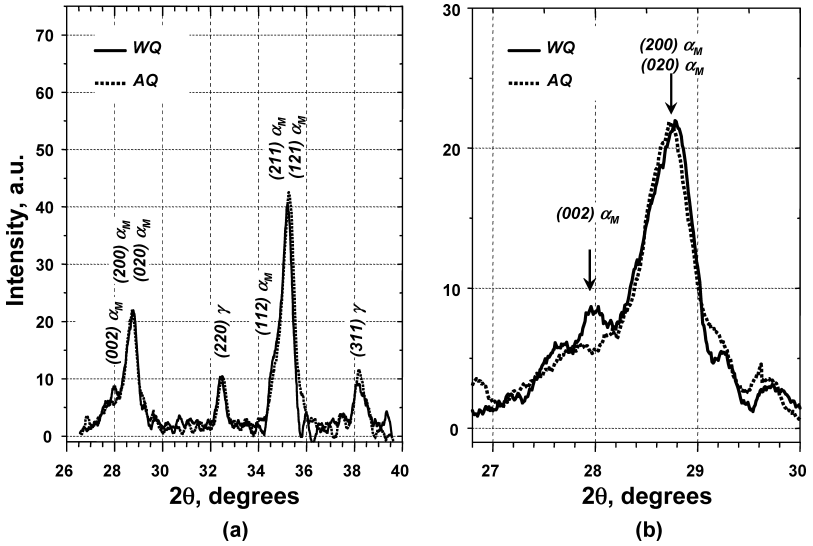

Fig. 4. Diffractogram for the WQ and AQ martensite: (a) 2θ range from 26° to 40°, (b) (200)α_M doublet in detail.

range. Therefore, at higher heating rates (>100°C/min), it is difficult to observe both mechanisms separately. A volume increase, as observed in stage IV, can be expected due to the transformation of retained austenite, which was originally reported[20] to transform to ferrite and θ-carbide, Fe_3C. In more recent work,[21] it was shown that the retained austenite transformed to ferrite and χ-carbide, Fe_2C_5. Work on the tempered martensite embrittlement phenomenon in structural steels has shown that the austenite decomposition leads to a microstructure comparable to upper bainite.[20] During the austenite transformation, the η-transition carbide may also transform into Hägg-carbide. Both phenomena together are usually referred to as the "second stage" of martensite tempering.

Stage V results in a further decrease of the martensite volume of about 0.30 vol%. This stage is commonly referred to as the third and final stage of the martensite tempering. It leads to the formation of θ-carbide, Fe_3C, and a cubic martensite matrix.

4. Discussion

Additional information on the different tempering process stages was gathered by means of XRD measurements and isothermal dilatometric tests. The observed volume changes during the latter tests were correlated with the expected volume changes based on the available crystallographic data.

4.1. XRD Measurements

In order to verify the different stages and mechanisms leading to the observed volume changes during martensite tempering, XRD measurements were carried out. The samples were specifically chosen to obtain XRD data after each of the stages observed during the heating experiments are reviewed in **Table 3**.

In order to investigate the occurrence of the auto-tempering of the martensite during cooling, XRD data of water-quenched (WQ quench rate: 500°C/s) and air-quenched (AQ quench rate: 10°C/s) martensite were compared. The results are shown in **Fig. 4**. The XRD results are very similar, but a significant difference can be seen clearly in the (002)α_M peak. The intensity of the (002)α_M peak and the $c_{\alpha_M}/a_{\alpha_M}$ ratio are both smaller for the air-quenched sample. These changes are a clear indication of segregation and/or cluster formation in the AQ sample as a result of auto-tempering. Using the $c_{\alpha_M}/a_{\alpha_M}$ ratio, the decrease of the solute carbon content due to auto-tempering was estimated to be 0.1 mass%.

Figure 5 shows the XRD results for stages I and II. The most significant results are summarized in Table 3. Martensite doublet peaks are clearly observed for the

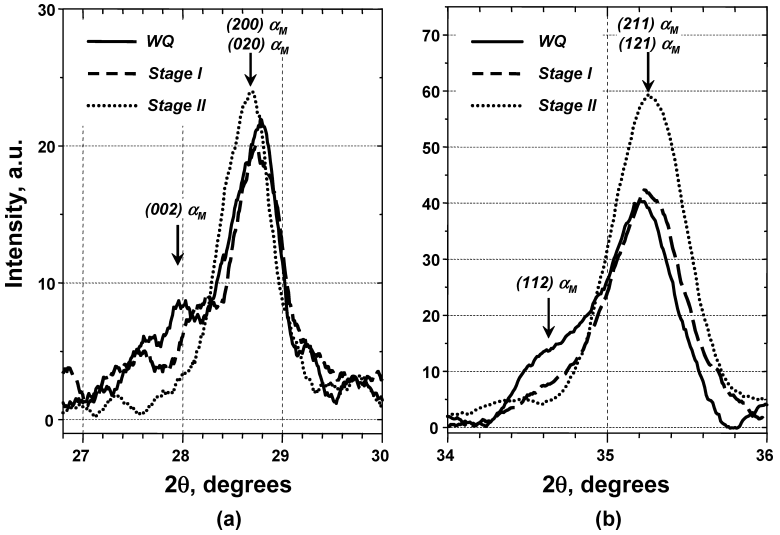

Fig. 5. Diffractogram of the martensite, in the as-quenched state (WQ), and after stages I and II: (a) (200)α_M doublet and (b) (211)α_M doublet.

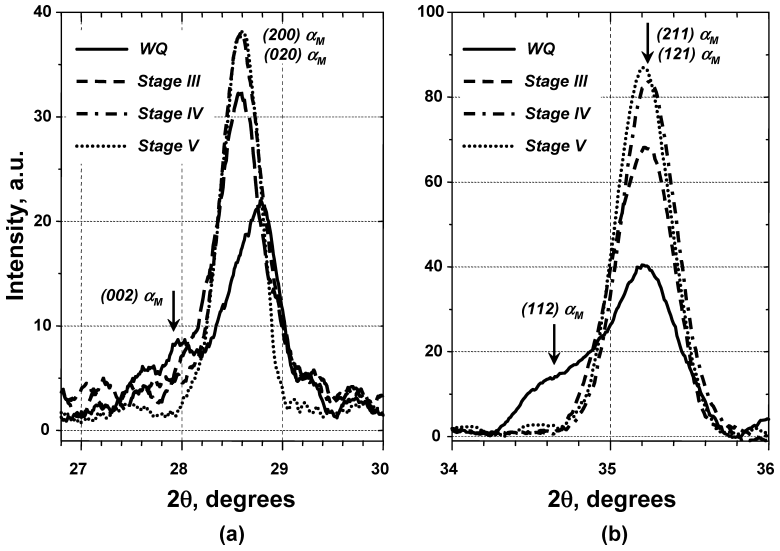

Fig. 6. Diffractogram of the martensite, in the as-quenched state (WQ), and after stages III, IV and V: (a) (200)α_M doublet and (b) (211)α_M doublet.

quenched specimen. Using the same peak deconvolution method as for the neutron diffraction measurements,[4] c_{α_M} and a_{α_M} could be determined. The XRD measurement also revealed that the quenched sample contained 15.2 % of retained austenite.

The stage I sample contained about 0.22 mass% less carbon than the WQ sample due to segregation, and this is the most likely reason for the first small volume decrease observed in the dilatometer experiments. Segregated carbon atoms do not contribute to the tetragonality of the martensite lattice. This results in a smaller $c_{\alpha_M}/a_{\alpha_M}$ ratio. The amount of austenite did not change.

For the stage II sample, the $c_{\alpha_M}/a_{\alpha_M}$ ratio approaches 1. The tempered martensite has almost completely lost its tetragonality, strongly suggesting that the interstitial carbon is involved in the formation of low-temperature transition carbides. No direct proof for these transition carbide precipitates was found in the diffractograms, since the sensitivity of the technique is inadequate. The existence of the precipitates was, however, already clearly shown by previous neutron diffraction measurements.[4] Finally, a slight decrease in the amount of retained austenite is also observed.

In the results for the stage III sample, shown in **Fig. 6**, the martensite doublet becomes a single peak as a result of the absence of solute carbon. The amount of retained austenite remains high.

The austenite peaks are absent after the stage IV heating treatment. This confirms that the small volume increases observed during both heating and isothermal experiments indeed result from the decomposition of the retained austenite.

As the presence of carbides could not be detected using XRD measurements, no additional changes were observed for the stage V sample by XRD.

4.2. Isothermal Dilatometric Tests

Isothermal tempering tests carried out in the dilatometer in the temperature range of 50–170°C were performed in order to observe the volume changes associated with segregation and η-carbide precipitation only. The transformation

rate of the tempering phenomena for two different tempering temperatures is shown in **Fig. 7**. It is worth noticing that for temperatures higher than 80°C the volume change already started before the isothermal holding temperature was reached. A correction was made in that case to take into account the changes occurring during heating to the isothermal temperature. The evolution of the volume change was fitted to the JMA equation (Eq. (2)). If the transformation mechanism is unique, a plot of $\ln(\ln(1/(1-f)))$ *vs.* $\ln(t)$ results in a single straight line with a slope equal to n and an intersection with the *Y*-axis equal to $n \cdot \ln(k)$. It can be observed that $\ln(\ln(1/(1-f)))$ is described by two straight line segments for temperatures up to 80°C. This strongly suggests that at least two different mechanisms cause the volume decrease during the low temperature tempering. The intersection of the two line segments occurs at shorter annealing times for an increasing tempering temperature.

Using the Arrhenius-type equation (Eq. (3)), the activation energy, related to both tempering mechanisms, was calculated from the *k*-values as shown in **Fig. 8**. The kinetic data of both observed tempering phenomena are summarized in **Table 4**.

According to Cottrell, the kinetics of the diffusion of carbon atoms to dislocations in a ferritic matrix follows a $t^{2/3}$-law. The observed *n*-value of 0.67 for stage I of tempering on the one hand strongly suggests that carbon segregation causes the first volume decrease of the martensite. Furthermore, the activation energy (98.9 kJ/mol) is only very slightly larger than literature values reported for carbon segregation as reviewed in **Table 5.**[1,2,22,23]

The low *n*-value (0.39) obtained for stage II of tempering on the other hand strongly suggests that the volume change is diffusion-controlled. In a study devoted to the tempering of Fe–Ni–C–martensite, Sherman *et al.*[24] proposed that Fe-diffusion along dislocations is the rate-determining step for η-carbide precipitation. The observed activation energies for this stage are (120–127 kJ/mol) indeed close to the activation energy associated with dislocation pipe-diffusion of iron, 134 kJ/mol[2,5].

Figure 9 shows the volume increase due to the decomposition of retained austenite during stage V, in the temperature range of 200–350°C. Despite the volume decrease resulting from the formation of transition carbides, a small volume increase was noticed for isothermal holding at 250°C.

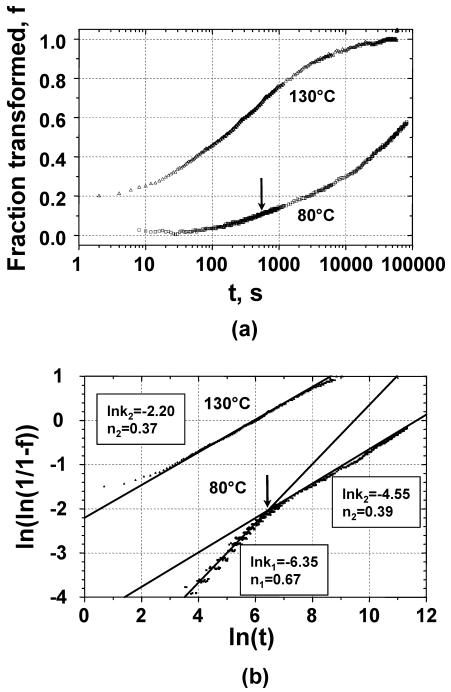

Fig. 7. Evolution of the volume decrease due to 80°C and 130°C tempering treatments (a). $\ln(\ln(1/(1-f)))$ plots for the same tempering temperatures (b).

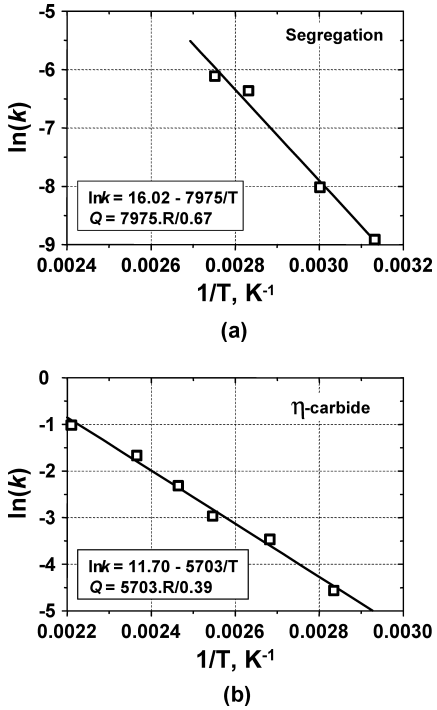

Fig. 8. The $\ln(k)$ *vs.* $1/T$ plot for the determination of the activation energy of the different tempering stages based on Eq. (10).

Table 5. Activation energies for carbon segregation.

Material	Activation energy	Ref.
α-Fe	84.1 kJ/mol	21)
Fe-C Martensite	83.0 kJ/mol	22)
ULC Steel	85.6 kJ/mol	1,2)
DP Steel	98.9 kJ/mol	Present work

Table 4. Kinetic data of the low temperature tempering phenomena, based on isothermal tests.

	Phenomenon	Activation Energy Q	n-value	Temperature range
I	C-segregation to lattice defects	98.90 kJ/mol	0.67	50-90°C
II	η-carbide precipitation	121.6 kJ/mol	0.39	80-180°C

4.3. Crystallography Based Specific Volumes

The volume effects observed in dilatometry due to the stages of tempering could be estimated using the crystallographic data presented in **Table 6**.

Two major steps in the martensite volume decrease were experimentally identified. The first one, corresponding to stage II, was associated with a relative volume decrease of $100 \cdot \Delta V/V = 0.31$–$0.38$ vol%.

The relative volume change of the martensitic phase, $\Delta V/V$, could be ascribed to the following processes:

$$\alpha_M \rightarrow \alpha_S + \varepsilon \quad \text{or} \quad \alpha_M \rightarrow \alpha_S + \eta$$

The associated relative volume changes are given by:

$$\frac{\Delta V}{V} = \frac{(100-(1+y)\cdot C_T + y\cdot C_S)\cdot V_{\alpha_S} + y\cdot(C_T - C_S)\cdot V_{\varepsilon/\eta} - (100-C_T)\cdot V_{\alpha_M}}{(100-C_T)\cdot V_{\alpha_M}} \quad \text{.....(6)}$$

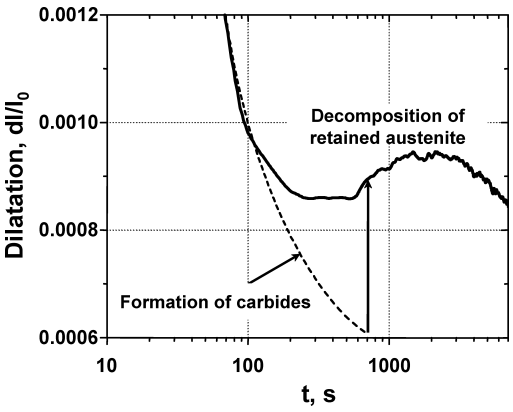

Fig. 9. Isothermal holding dilatation curve at 250°C, which reveals the decomposition of the retained austenite.

Where α_M denotes martensite, α_S the ferrite containing segregated carbon, C_T and C_S, the total and segregated carbon in at%, V_i, the volume per Fe-atom of constituent i and y is the Fe/C atomic ratio in the transition carbide. Based on literature data, the atom ratio for the transition-carbides, is 2 for η-carbide (Fe_2C)[29] and 2.4 for ε-carbide ($Fe_{2.4}C$).[19, 28]

The results of the calculations are shown in **Table 7**. C_T is equal to 3.24 at% C, based on the composition listed in Table 1. The amount of segregated carbon, C_S, is equal to 1 at% C, or approximately 0.2 mass% C, and for y, values of 2 and 2.4 were taken as atom ratios found for the transition carbide. A good agreement between the experimental and calculated volume decrease was found for a y-value of 2.4. Consequently, the best agreement with the present results was obtained for the formation of ε-carbide, rather than η-carbide.

Table 7. Calculated volume effects after stage II of tempering for the martensite.

Reaction	η (Fe_2C) ΔV/V, %	ε ($Fe_{2.4}C$) ΔV/V, %	Experimental ΔV/V, %	Ref.
$\alpha_M \longrightarrow \alpha_S + \varepsilon$	-0.583	-0.397	- (0.31 – 0.38)	28)
$\alpha_M \longrightarrow \alpha_S + \varepsilon$	-0.673	-0.505		19)
$\alpha_M \longrightarrow \alpha_S + \eta$	-0.546	-0.353		29)

Table 6. Crystallographic data for the different constituents.

Constituent	Lattice parameters, nm	Fe atoms per unit cell	Volume per Fe atom, nm³	Ref.
bct α_M	a = 0.2866 - 0.0013 · mass% C c = 0.2866 + 0.0116 · mass% C	2	$12.04 \cdot 10^{-3}$ if mass% C = 0.72	26)
bcc α-Fe	a=0.2866	2	$11.78 \cdot 10^{-3}$	27)
fcc γ-Fe	a = 0.3555 + 0.0044 · mass% C	4	$11.54 \cdot 10^{-3}$ if mass% C = 0.72	28)
hcp ε ($Fe_{2.4}C$)	a=0.2752 c=0.4353	2	$14.28 \cdot 10^{-3}$	29)
hcp ε ($Fe_{2.4}C$)	a=0.2735 c=0.4335	2	$14.04 \cdot 10^{-3}$	19)
orthorhombic η (Fe_2C)	a=0.4704 b=0.4318 c=0.2830	4	$14.37 \cdot 10^{-3}$	30)
orthorhombic θ (Fe_3C)	a=0.4523 b=0.5088 c=0.6743	12	$12.93 \cdot 10^{-3}$	31)

A second large reduction of the volume took place in the temperature range between 200°C and 400°C. The total length change for the completed tempering phenomena (0.62–0.71 vol%), occurring in the martensite, is the result of two main transformations: the decomposition of martensite to a mixture of ferrite and cementite and the decomposition of austenite to the same type of mixture. A theoretical prediction of the total relative volume change was obtained from:

$$\alpha_{\mathrm{M}} \rightarrow \alpha + \vartheta$$

$$\frac{\Delta V}{V} = \frac{(100-4\cdot C_{\mathrm{T}})\cdot V_{\alpha} + 3\cdot C_{\mathrm{T}}\cdot V_{\theta} - (100-C_{\mathrm{T}})\cdot V_{\alpha_{\mathrm{M}}}}{(100-C_{\mathrm{T}})\cdot V_{\alpha_{\mathrm{M}}}} \quad \text{.....(7)}$$

and

$$\gamma \rightarrow \alpha + \vartheta$$

$$\frac{\Delta V}{V} = \frac{(100-4\cdot C_{\mathrm{T}})\cdot V_{\alpha} + 3\cdot C_{\mathrm{T}}\cdot V_{\theta} - (100-C_{\mathrm{T}})\cdot V_{\gamma}}{(100-C_{\mathrm{T}})\cdot V_{\gamma}} \quad \text{.....(8)}$$

Using the crystallographic data of Table 6, the relative volume changes corresponding to the above reactions were calculated for martensite containing 0.72 mass% C:

$$\alpha_{\mathrm{M}} \rightarrow \alpha + \vartheta \qquad \frac{\Delta V}{V} = -1.228\,\% \quad \text{.....(9)}$$

$$\gamma \rightarrow \alpha + \vartheta \qquad \frac{\Delta V}{V} = +3.093\,\% \quad \text{.....(10)}$$

As the martensite contained 12 % of retained austenite, a total volume decrease $\Delta V/V$ of 0.71 %, *i.e.*, $(0.12\cdot 3.093 - 0.88\cdot 1.228)$, is predicted. This value agrees with the observed volume changes, which was in the range of 0.62–0.71 %. It is worth noticing that the decomposition of retained austenite leads to an increase of length of the specimen. The predicted volume increase amounts to 0.371 %. The observed length increase was smaller because the decomposition of retained austenite occurred at the same time as the formation of the transition carbides.

5. Conclusions

Five different stages were distinguished during the tempering of quenched martensite similar to the martensite phase present in DP steel in the temperature range of 20°C–500°C.

Stage I: The redistribution of carbon atoms takes place during ageing below 120°C. Carbon segregation induces a modest volume change of less than 0.05 vol% and a significant reduction of the tetragonality of the martensite lattice. The activation energy was determined to be 98.9–100.6 kJ/mol, corresponding to the activation energy for volume diffusion of carbon.

Stage II: The precipitation of η- or ε-carbide in the 120–200°C temperature range yields an activation energy of 121.6–123.8 kJ/mol, and suggests a rate control by diffusion of iron atoms along dislocations to accommodate the volume misfit between the carbide and the matrix. The precipitation causes a volume decrease of about 0.30 vol%. It also results in the loss of tetragonality of the martensite lattice.

Stage III: An activation energy of 135.8 kJ/mol is found for Hägg-carbide precipitation, which followed the precipitation of η-carbide in the 200–300°C temperature range.

Stage IV: The only tempering process that results in a volume increase is the decomposition of retained austenite in the 250–350°C temperature range. The activation energy was found to be 154.7 kJ/mol.

Stage V: In this final stage, all transition carbides, present in the martensite, transform into cementite at sufficiently high temperatures (290–390°C), this process has an activation energy of 176.1 kJ/mol.

A total volume decrease of 0.62–0.71 vol% is found after full tempering.

REFERENCES

1) A. K. De, S. Vandeputte and B. C. De Cooman: *Scr. Mater.*, **41** (1999), 831.
2) A. K. De, S. Vandeputte and B. C. De Cooman: *Scr. Mater.*, **44** (2001), 695.
3) T. Waterschoot, A. K. De, S. Vandeputte and B. C. De Cooman: *Metall. Mater. Trans. A*, **34A** (2003), 781.
4) T. Waterschoot, S. Vandeputte, B. C. De Cooman and K. Conlon: *Z. Metallkd.*, **94** (2003), 424.
5) A. H. Cottrell and B. A. Bilby: *Proc. Phys. Soc.*, **A62** (1949), 49.
6) E. J. Mittemeijer, A. van Gent and P. J. van der Schaaf: *Metall. Trans. A*, **17** (1986), 1441.
7) E. J. Mittemeijer, L. Cheng, P. J. van der Schaaf, C. M. Brakman and B. M. Korevaar: *Metall. Trans. A*, **19A** (1988), 925.
8) L. Cheng, C. M. Brakman, B. M. Korevaar and E. J. Mittemeijer: *Metall. Trans. A*, **19A** (1988), 2415.
9) L. Cheng, N. M. van der Pers, A. Böttger, T. H. de Keyser and E. J. Mittemeijer: *Metall. Trans. A*, **22A** (1991), 1957.
10) B. D. Cullity: Elements of X-Ray Diffraction, 2nd Ed., Addison-Wesley Publishing Co, Inc., Boston, MA, (1978), 508.
11) G. R. Speich: *Trans. AIME*, **245** (1969), 2553.
12) G. R. Speich and W. C. Leslie: *Metall. Trans. A*, **3A** (1972), 1043.
13) G. R. Speich and R. L. Miller: Fundamentals of Dual Phase Steels, AIME, New York, NY, (1981), 279.
14) D. P. Koistinen and R. E. Marburger: *Acta Metall.*, **7** (1959), 59.
15) O. N. C. Uwakweh, J.-M. R. Génin and J.-F. Silvain: *Metall. Trans. A*, **22** (1991), 797.
16) C. S. Roberts, B. L. Averbach and M. Cohen: *Trans. Am. Soc. Met.*, **45** (1953), 576.
17) B. S. Lement, B. L. Averbach and M. Cohen: *Trans. Am. Soc. Met.*, **46** (1954), 851.
18) F. E. Werner, B. L. Averbach and M. Cohen: *Trans. Am. Soc. Met.*, **49** (1957), 823.
19) B. S. Lement, B. L. Averbach and M. Cohen: *Trans. Am. Soc. Met.*, **47** (1955), 291.
20) K. H. Jack: *J. Iron Steel Inst.*, **169** (1951), 26.
21) C. B. Ma, T. Ando, D. L. Williamson and G. Krauss: *Metall. Trans. A*, **14** (1983), 1033.
22) C. A. Wert: *Phys. Rev.*, **79** (1950), 601.
23) P. C. Chen and P. G. Winchell: *Metall. Trans. A*, **11** (1980), 1333.
24) A. M. Sherman, G. T. Eldis and M. Cohen: *Metall. Trans. A*, **14** (1983), 995.
25) M. Cohen: *Trans. JIM.*, **11** (1970), 145.
26) P. G. Winchell and M. Cohen: *Trans. Am. Soc. Met.*, **55** (1962), 347.
27) R. C. Ruhl and M. Cohen: *Trans. AIME*, **245** (1969), 241.
28) C. S. Roberts: *Trans. AIME*, **197** (1953), 203.
29) S. Nagakura: *J. Phys. Soc. Jpn.*, **14** (1959), 186.
30) Y. Hirotsu and S. Nagakura: *Acta Metall.*, **20** (1972), 645.
31) Powder diffraction file, ASTM card, 6-0688.